Received: 22 May 2019 | Revised: 20 June 2019 | Accepted: 20 June 2019

DOI: 10.1111/jace.16661

ORIGINAL ARTICLE

Journal of the American Ceramic Society

Thermal activation effects in crack propagation and reliability of fused silica

Robert F. Cook

Materials Measurement Science Division, National Institute of Standards and Technology, Gaithersburg, Maryland

Correspondence
Robert F. Cook, Materials Measurement Science Division, National Institute of Standards and Technology, Gaithersburg, MD 20899.
Email: robert.cook@nist.gov

Abstract

The thermal activation energy u_1 characterizing changes in crack velocity with temperature for fused silica in water is determined. The determination is based on a new analysis that incorporates the familiar Arrhenius term for thermally activated processes and a term characterizing the departure of the propagating crack system from fracture equilibrium. In determining u_1 from experimental data, the Arrhenius term and the nonequilibrium term are of approximately equal magnitude. The analysis is applied to an extensive compilation of crack velocity measurements in fused silica to arrive at an estimate of $u_1 = (69 \pm 11)$ kJ mol^{-1}, where the value represents the multi-laboratory mean ± variability. This value is greater than that assumed in some earlier works and characterizes a typical within-laboratory increase in crack velocity of a factor of approximately 10^2 in fused silica between freezing and boiling water conditions and a decrease of a factor of 10^3 in component time to failure for the same change in conditions. The multi-laboratory variation in velocity at fixed temperature is comparable to the within-laboratory maximum increase, perhaps obscuring temperature effects.

KEYWORDS

glass, fracture, thermal properties

1 | INTRODUCTION

In a recent work considering ceramic reliability controlled by fracture,[1] the claim was made that thermal effects are small. More specifically, the claim and analysis presented suggested that changes in temperature had only small direct effects on crack propagation velocities and therefore on lifetimes of stressed ceramic components. Changes in temperature were noted to have large indirect effects on crack propagation and thence lifetime only though thermal expansion-mediated influences on stress and crack driving force. It was concluded that the accelerating effects of temperature cycling or high temperature exposure on time to failure, as often implemented in commercial practice to assess reliability, were dominated by the stress changes generated in components rather than by changes in underlying material crack velocity behavior.

The claim was based on the selection of a small value, 0.15 eV, 14.5 kJ mol^{-1}, for the characteristic energy barrier for thermally activated bond rupture and crack propagation, consistent with measurements on a range of ceramic materials in water.[2] The success rate of crack tip bond configurations passing over energy barriers for bond rupture increases as temperature increases, and thus crack advance is more rapid. However, for a fixed temperature increase, rate processes are exponential functions of barrier height, and thus a small barrier leads to small velocity increases and small effects of temperature on lifetime and reliability. It is the contention of the work here that the earlier claim and selection of activation energy are not universal. In fact, it will be demonstrated

that fused silica glass has a relatively large thermal activation energy characterizing crack propagation in water, leading to significant direct effects of temperature on crack velocity and component lifetime and reliability. Fused silica is the major constituent of optical fibers for advanced communications and a critical insulating and etch-resistant element in microelectronic devices and microelectromechanical systems (MEMS) sensors and actuators. In addition, fused silica is a basis for consideration of fracture in other glasses, such as those used in digital display panels or even cookware. Hence, accurate quantitative prediction of temperature effects in reliability of fused silica is of great commercial importance.

The work here begins with an outline of the analysis, originally developed by Lawn,[3] and subsequently refined and implemented to describe thermally activated crack propagation in glasses,[4] ceramics,[2,5] organic-inorganic hybrid thin films,[6] metal-oxide interfaces,[7] and most recently in consideration of reliability.[1] A new formulation is then developed from the analysis that enables the thermal activation energy to be determined from crack velocity measurements as a function of temperature: Significantly, it is not simple Arrhenius behavior. The formulation is applied to an extensive set of data taken from the somewhat diverse published literature and rendered into appropriate and consistent form. These data also serve as a review of crack velocity measurements in fused silica. Estimates of the major crack velocity parameters and their uncertainties are generated for fused silica based on this data set. The parameters and uncertainties are then used in a demonstration of the effects of temperature on component lifetime. The conclusion enumerates the determined temperature-independent parameters.

2 | ANALYSIS

A general nonequilibrium crack expansion rate for a fracture system driven by mechanical energy release rate G is

$$\mathrm{d}A/\mathrm{d}t = \dot{A}_0 \sinh\left[(G-2\gamma)/\eta\right], \tag{1}$$

where A is crack area, t is time, and

$$\begin{aligned} 2\gamma &= u_0/a^2 \\ \eta &= 2kT/a^2 \\ \dot{A}_0 &= \left(2kTa^2/h\right)\exp\left(-u_1/kT\right) \end{aligned} \tag{2}$$

The terms 2γ, η, and $\dot{A}_0$ in Equation (1) are macroscopic crack propagation parameters, all of which depend through Equation (2) on fundamental nanoscale bond rupture parameters, a, u_0, and u_1, and two of which depend on temperature, T (k is Boltzmann's constant, h is Planck's constant). The parameter u_0 is the energy required to break a single bond of the material in the crack propagation environment and a^2 is the incremental bond area. The parameter 2γ is then recognized as the material fracture surface energy. For $G = 2\gamma$ the fracture system is in equilibrium and the crack propagation rate is zero[8] and 2γ is hence known as the crack velocity threshold. Thermal effects enter in three ways: (i) The parameter η is the thermal energy per bond area. (ii) The term kT/h appears in the first part of the expression for $\dot{A}_0$ (in parentheses) and is a characteristic thermal frequency. (iii) The parameter u_1 is the energy barrier separating incremental bond rupture states and appears in the second (exponential) term in $\dot{A}_0$. The parameter u_1 is part of an Arrhenius expression that depresses the crack expansion rate from the maximum value set by the characteristic frequency and incremental bond area to decreased values with decreasing temperature.

Equations (1) and (2) are modified for experimental measurements of crack propagation along a single dimension c, the crack length, with crack velocity $v = \mathrm{d}c/\mathrm{d}t$. Combining this definition with Equations 1 and 2 gives.

$$v = v_0 \sinh\left[(G-2\gamma)/\eta\right]/B, \tag{3}$$

where

$$v_0 = (2kTa/h)\exp\left(-u_1/kT\right) \tag{4}$$

and $B = (s/a)$ is the ratio of the effective crack periphery s and the bond separation a. For straight cracks B is a constant, although s may be less than the specimen width if not all bond sites along a crack front are active. Equation (3) may then be seen to partition crack velocity into a kinetic term v_0, a nonequilibrium, thermally scaled crack driving term $(G-2\gamma)/\eta$, and a geometry term B. If the fracture system is far from equilibrium such that $G \gg 2\gamma$, Equation (3) reduces to

$$v = v_\mathrm{A}\exp(G/\eta), \tag{5}$$

where v_A is a velocity that contains kinetic, geometry, and surface energy dependence from Equation (3). Full details and discussions of crack velocity behavior are given elsewhere.[1–6,8]

In this work, a major application of the above analysis is evaluation of the thermal activation energy u_1 from experimental $v(G)$ observations. A fracture system is considered in which the crack velocity is measured at fixed mechanical energy release rate and variable temperature (this will be seen below to be the reverse of normal practice). For a straight crack at two different temperatures, T_i and T_j, two different crack velocities, v_i and v_j, are observed. From Equations (2), (3), and (4),

$$v_i = \left(2kT_ia/h\right)\exp\left(-u_1/kT_i\right)\sinh\left[(G-2\gamma)a^2/2kT_i\right]/B \tag{6a}$$

and

$$v_j = \left(2kT_ja/h\right)\exp\left(-u_1/kT_j\right)\sinh\left[(G-2\gamma)a^2/2kT_j\right]/B, \tag{6b}$$

noting that the bond rupture parameters a and u_0, and therefore 2γ, are temperature invariant. Far from equilibrium, Equation (6) becomes an expanded version (5):

$$v_i = \left(kT_i a/h\right) \exp\left(-u_1/kT_i\right) \exp\left[(G-2\gamma)\, a^2/2kT_i\right]/B \quad (7a)$$

and

$$v_j = \left(kT_j a/h\right) \exp\left(-u_1/kT_j\right) \exp\left[(G-2\gamma)\, a^2/2kT_j\right]/B. \quad (7b)$$

The geometry term B can be eliminated between Equations (7a) and (7b) to give an expression for u_1 as three terms:

$$u_1 = k\left(\frac{1}{T_j}-\frac{1}{T_i}\right)\ln\left(\frac{v_i}{v_j}\right)+(G-2\gamma)\, a^2/2 + k\left(\frac{1}{T_j}-\frac{1}{T_i}\right)\ln\left(\frac{T_j}{T_i}\right). \quad (8)$$

The first term in Equation (8) is the familiar Arrhenius expression relating a change in a rate, crack velocity here, to a change in temperature. The second term recognizes that the system must be perturbed from equilibrium to generate a crack velocity[8] and will be seen to be a major factor here. The third term recognizes that the crack propagation process is thermally activated from a characteristic thermal frequency. The importance of Equation (8) is that it provides a clear quantitative method for evaluation of u_1 based on fundamental crack propagation kinetics, from Equations (1) to (7). The focus here is on fused silica in water and hence T_i and T_j are restricted to the domain 273 to 373 K (0°C-100°C); the logarithmic third term in Equation (8) is thus expected to be small. Conversely, most crack velocity measurements in fused silica are sufficiently removed from equilibrium that the second, nearly always neglected, $(G-2\gamma)$ term in Equation (8) is expected to be significant.

3 | CRACK PROPAGATION PARAMETERS

3.1 | Bond separation and surface energy

In determining the thermal activation energy using Equation (8), attention is first focused on evaluating the temperature invariant bond separation and surface energy parameters, a and 2γ. Combining Equations (2) and (5) and rearranging gives

$$\log(v) = \log\left(v_A\right) + [a^2/2\ln(10)\, kT]G, \quad (9)$$

showing that at fixed temperature far from equilibrium a semi-logarithmic $v(G)$ plot should exhibit straight line behavior with slope related to a. Figure 1 shows a comprehensive multi-laboratory composite plot of experimental crack velocity measurements for fused silica in water at approximately 25°C. The measurements cover a range of test configurations, mostly

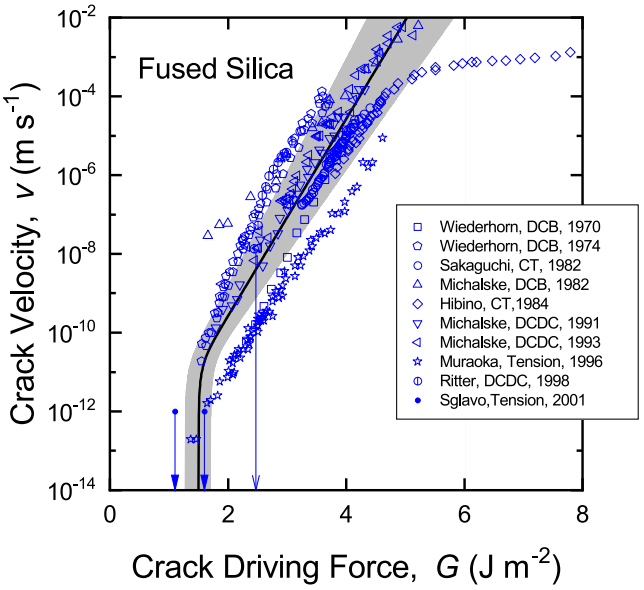

FIGURE 1 Compilation of crack velocity $v(G)$ measurements (symbols) and representative fit of model (Equation (3), line and shaded band). Measurements identified by first author, method, and year [Colour figure can be viewed at wileyonlinelibrary.com]

based on long crack geometries, including double cantilever beam (DCB), compact tension (CT), double cleavage drilled compression (DCDC), and fiber tension, and extend over nearly 50 years, including the early DCB experiments of Wiederhorn and colleagues,[9,10] the CT experiments of Sakaguchi et al,[11] the DCB and DCDC experiments of Michalske and colleagues[12–14] (also in other reports[15,16]), the CT experiments of Hibino and colleagues[17] (also in a preliminary report[18]), the fiber tension experiments of Muraoka et al,[19] and the DCDC experiments of Ritter et al.[20] The open symbols in Figure 1 represent individual v measurements digitized from published works, converting crack driving force reported as a stress-intensity factor, K, to $G = K^2/E$, where $E = 72$ GPa is the plane stress Young's modulus of fused silica.[21] Different symbols represent the different studies listed. The major, striking, feature of Figure 1 is the agreement between data from the different studies with regard to slope suggested by Equation (9). The data exhibit small differences in the implied v_A intercept term, probably caused by experimental geometry variations. However, over eight orders of crack velocity, from about $v = 10^{-12}$ to 10^{-4} m s^{-1}, the $v(G)$ trend is consistent with Equation (9) and a single underlying a value. A visual best fit using Equation (9) to represent the mean slope of the multi-laboratory data for the domain $v > 10^{-10}$ m s^{-1} is shown in Figure 1 as a solid line. The slope parameter (Equation 5) is $\eta = 0.174$ J m^{-2} and the range of the experimental data about the mean response suggest representative relative uncertainties of about ± 15% in the slope and intercept terms, shown as the shaded band. The resulting bond separation and uncertainty is $a = (0.218 \pm 0.016)$ nm (Equation 2). Note that here and throughout, the solid line and shaded band

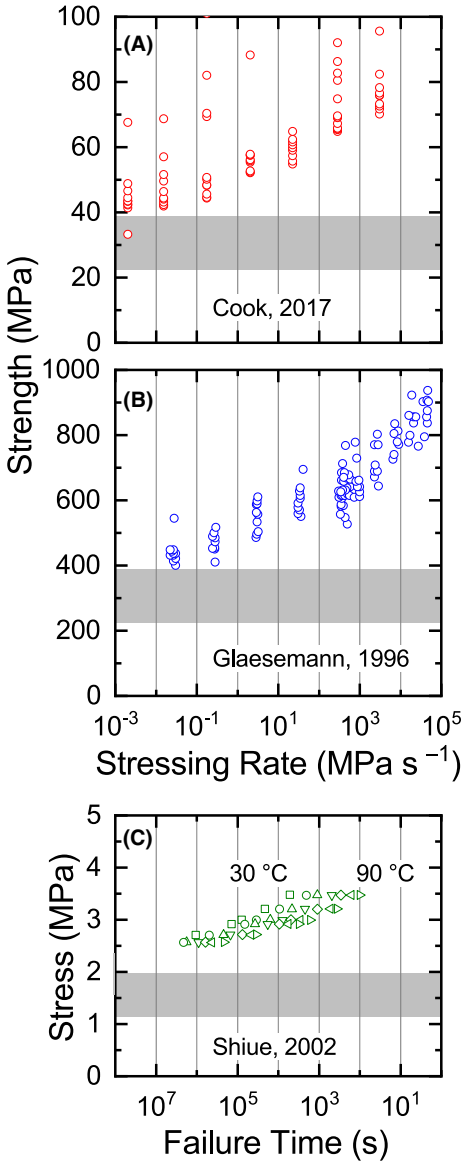

FIGURE 2 Measurements of failure stress vs stressing rate (A), (B) and stress vs failure time (C) for fused silica in water (symbols) and predicted lower bounds to stress (shaded bands). Measurements identified by first author and year. Different symbols represent different temperatures in (C) [Colour figure can be viewed at wileyonlinelibrary.com]

are representations of the typical response and variation about the response from multi-laboratory observations; the lines and bands do not result from statistical estimates of quantities and uncertainties (in this case, of the slope).

Another clear feature in Figure 1 is the CT data of Hibino et al[17] For mechanical energy release rate $G > 5$ J m^{-2}, these data exhibit a clear deviation from the overall straight line trend with increasing G to suppressed, almost constant, crack velocities, $v \approx 10^{-4}$ m s^{-1}. Such behavior is associated with transport-limited crack propagation, rather than reaction-limited propagation as considered here, and has been well characterized in fused silica crack velocity studies with varying temperature (see below) and humidity.[17,18] Such $v(G)$ behavior can be modeled as a process of water vapor diffusion along constricted cracks[4,7,22] leading to suppressed velocities. $G \approx 5$ J m^{-2} thus provides an approximate upper limit of applicability of the current model. Two other features in Figure 1 also illustrate known phenomena but are somewhat subtler. These are the DCB data of Wiederhorn et al[10] and the fiber tension data of Muraoka et al,[19] which lie above and below the shaded band, respectively. In the first case, the data illustrate increased crack velocities exhibited by glasses that contain cations other than Si (the glass studied by Wiederhorn et al contained some Ti and $E = 68$ GPa was used[21]). In the second case, the data illustrate decreased crack velocities exhibited by glasses in limited water (the experiments of Muraoka et al were conducted in 60% relative humidity environments). The DCDC experiments of Koike and colleagues conducted in 50% relative humidity[23,24] and the thin film experiments of Hatty et al conducted in air[25] generated velocities somewhat comparable to those in Figure 1 but are not included here as heat treatments likely altered the glass structures.

A feature that is almost absent from Figure 1 is clear appearance of the crack velocity threshold. In many glasses,[3,9,20,26] ceramics,[2,5,27] hybrid materials,[6,28] and interfaces,[7,20,28] crack velocity measurements exhibit an obvious, measurable, decrease toward zero crack velocity at a nonzero mechanical energy release rate. The nonzero value is known as the threshold as $v \to 0$ as $G \to 2\gamma$, and the full reaction-controlled $v(G)$ behavior is well described by Equation (3). Explicit crack velocity threshold measurements in fused silica are rare: The downward open-head arrow in Figure 1 shows a threshold, about 2.5 J m^{-2}, observed in the DCDC measurements of Ritter et al[20] The downward closed-head arrows show the range of thresholds, about 1.1 to 1.6 J m^{-2}, observed in the tension experiments of Sglavo and Green.[29]

Information regarding the crack velocity threshold in fused silica, although not extremely obvious in Figure 1, can be found elsewhere. Crack healing behavior has been observed in fused silica at $G \approx 0.1$ J m^{-2},[30,31] placing a weak absolute lower bound on the threshold. The most important additional threshold information, however, derives from fused silica strength and failure studies. As noted elsewhere,[1] threshold effects are more apparent in constant stress, or, particularly, constant stressing rate failure experiments. In constant stressing rate studies at very small applied stressing rates, the failure strength approaches an invariant lower bound related to the threshold. In constant stress studies, the failure time diverges as the applied stress approaches an analogous lower bound. For failure controlled by contact flaws, as is common in such tests, the lower bound reactive strengths are related to the upper bound inert strengths by the ratio $(2\gamma/2\gamma_0)^{2/3}$, where $2\gamma_0$ is the surface energy of the material in an inert environment.[32]

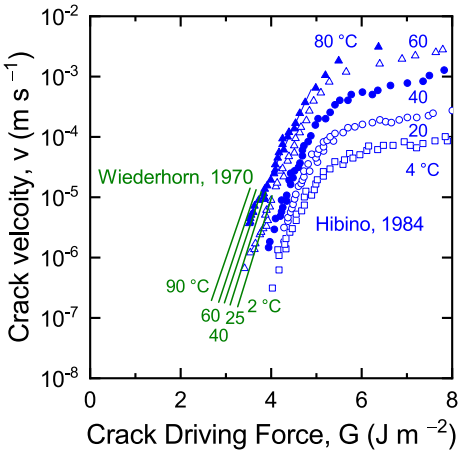

FIGURE 3 Crack velocity $v(G)$ measurements for fused silica in water as a function of temperature. Note the increase in velocity with temperature. Measurements identified by first author and year [Colour figure can be viewed at wileyonlinelibrary.com]

For fused silica[21] $2\gamma_0 = 8.8$ J m^{-2} and hence the strength ratio should be about 0.25 to 0.43 using the 2γ estimates from above. Figure 2 shows three sets of failure experiments for fused silica demonstrating threshold behavior and consistency with the estimated strength ratio. The vertical lines are a guide to the eye and the shaded bands are predictions of lower bound reactive strength plateau using the ratio range given above and the appropriate inert strengths. Figure 2A shows constant stressing rate results for indented fused silica disks in water at room temperature. Symbols represent individual strength measurements at the stressing rates indicated and are the "raw data" used previously.[32] The upper bound inert strength in these disk tests was about 90 MPa. Figure 2B shows constant stressing rate results for much stronger abraded optical fibers in water at room temperature. Symbols represent individual strength measurements and were digitized from published measurements by Glaesemann.[33] The upper bound near-inert strength in these fiber tests was about 900 MPa. In both Figure 2A,B, the strength data measured over seven orders of magnitude of stressing rate exhibit a clear tendency to lower bounds at small rates. The trend is not as definitive as some crystalline ceramic observations[2] but is clearly apparent, in qualitative agreement with expectation. More importantly, in quantitative agreement, extrapolations of the strength measurements to ultrasmall stressing rates lead to about 30% of the upper bounds, comparable to the predicted plateau values. Related measurements by Semjonov et al of abraded and zirconia-contaminated optical fiber in 50% relative humidity over 10 orders of magnitude of stressing rate exhibited a similar clear tendency at small rates to lower bound plateau strengths of 20%-40% of the upper bound.[34] Figure 2C shows constant stress failure data for untreated optical fibers at various temperatures in water. Symbols represent the means of about eight samples and were digitized from the published data of Shiue and Matthewson;[35] experimental variation is approximately the symbol size and the upper bound to the strength is about 5 GPa. Although for failure times extending over four orders of magnitude, a lower bound to the failure stress is not as apparent as in Figure 2A,B, the data display a clear tendency to time divergence consistent with the prediction. (Temperature effects are discussed below.)

Taken together, the crack velocity threshold observations, the failure stress plateau observations, and quantitative agreement between the two provide strong support for a fracture surface energy value for fused silica in water of $2\gamma = (1.50 \pm 0.23)$ J m^{-2}, using relative ± 15% uncertainty to describe experimental variation. The solid line and shaded band in Figure 1 use these values and Equation (3) to describe the $v(G)$ behavior over the full velocity range. The determined values of a and 2γ in Equation (2) give $u_0 = (43 \pm 13)$ kJ mol^{-1}.

3.2 | Thermal activation energy

Attention is now focused on evaluating the invariant thermal activation energy u_1 using Equation (8) and experimental sets of $v_i(T_i)$ and $v_j(T_j)$ pairs. Such sets were digitized and converted into a consistent format from the published DCB experiments of Wiederhorn and colleagues,[9,10] the CT experiments of Sakaguchi et al,[11] the CT experiments of Hibino et al,[17] and the DCDC experiments of Fisk and Michalske.[35] Figure 3 shows as symbols the variation of $v(G)$ responses observed as a function of temperature by Hibino et al[17] The data exhibit exponential trends at small values of G before tending to velocity plateau at large values of G. The effects of increasing T are to shift the exponential behavior to greater v and the onset of the plateau to greater G. Also shown as straight lines in Figure 3 are similar responses observed by Wiederhorn and Bolz.[9] These data are more restricted in range, exhibiting only an exponential trend, but also exhibit increases in v with increases in T. Other observations[10,11] were similar to these, or reported the increased ratio of observed velocities as a function of increased temperature.[36] Supporting evidence for thermally activated increases in crack velocity with temperature in fused silica is provided by decreased failure times in the constant stress failure data of Figure 2C[35] and earlier[37,38] and decreased strengths in constant stressing rate data.[38–42]

For each experimental data collection such as in Figure 3, a single value of G within the domain of exponential behavior was selected and the $v(T)$ behavior determined. For each distinct $v_i(T_i)$, $v_j(T_j)$ pair within a collection, Equation (8) was then used to estimate a value of u_1 using the value of G selected and the a and 2γ values determined above. The uncertainty in each u_1 estimate was determined from the uncertainties in the a and 2γ values, an assumed ±15% relative

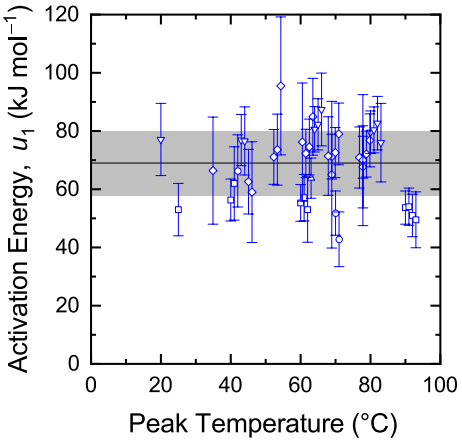

FIGURE 4 Estimates of thermal activation energy u_1 for crack propagation in fused silica in water (different symbols represent different laboratories) and multi-laboratory average and variation (line and shaded band, 69 ± 11 kJ mol^{-1}) [Colour figure can be viewed at wileyonlinelibrary.com]

uncertainty in each v, and no correlation between uncertainties. The values of u_1 so determined are shown in Figure 4, which plots the estimates and uncertainties as a function of the maximum temperature in a pair; some points are offset for clarity. There is no significant trend with temperature and the estimates from the wide range of sources[9–11,17,36] are in agreement. A conservative estimate of the thermal activation energy for crack velocity in fused silica may be made by separately averaging the estimates and uncertainties to give $u_1 = (69 \pm 11)$ kJ mol^{-1}, shown as the shaded band in Figure 4 encompassing most estimates.

The importance of using a complete formulation for u_1 that considers departure of the fracture system from equilibrium, Equation (8), and which thus requires the above quantitative evaluations of a and 2γ, is made clear in the relative contributions to the u_1 estimates. A typical estimate involved approximately 62% contribution from the first Arrhenius term, 42% contribution from the second nonequilibrium term, and −4% from the third frequency term, with similar relative contributions to the uncertainty. Hence, neglect of the second term, setting equilibrium $G = 2\gamma$ in Equation (8), would lead to significant underestimation of u_1, consistent with the reports of 43 and 20 kJ mol^{-1}.[17,36] Conversely, maximizing the second term by assuming zero threshold, setting $2\gamma = 0$ in Equation (8), would lead to significant overestimation of u_1, consistent with the reports of 139 and 127 kJ mol^{-1}.[9,10] In a related consideration, using Equation (7a) alone and not using Equation (8) to eliminate the unknown geometry term B led to underestimation of u_1 as B was overestimated: Setting $G = 2\gamma$ eliminates the second exponential term in Equation (7a) and using the experimentally reported value of B and a single $v(T)$ point led to the reported 53 kJ mol^{-1}.[5] A consequence was the small values of 10 to 40 kJ mol^{-1} reported for ceramics and other glasses,[2,4] which were in apparent agreement with the earlier reports of 55 kJ mol^{-1} for soda-lime glass.[43]

4 | RESULTS

4.1 | Crack velocity behavior

Figure 5 shows the $v(G)$ behavior for fused silica in water at various temperatures using Equation (3) and the crack velocity parameters determined from the above experimental observations. The lines in Figure 3 were calculated from the new analysis. The solid line is for $T = 25$°C, room temperature, and essentially replicates the "average response" line from Figure 1 within the domain of model applicability. The upper, dashed, line in Figure 5 is for $T = 100$°C, boiling water. The crack velocity increases substantially, about a factor of 10^2, with increase in temperature, reflecting the exponential dependence on the calibrated, large, thermal activation energy. The dependence of the crack velocity on the mechanical energy release rate decreases slightly, reflecting the simple inverse dependence on the thermal energy per bond. The changes in the $v(G)$ response on increasing the temperature from 25°C to 100°C as indicated by the solid and dashed lines in Figure 5 reflect the expected *within*-laboratory behavior and are consistent with observations, for example, Figure 3. However, the variability in the observed thermal activation energies, Figure 4, leads to considerable uncertainty in *between*-laboratory comparison of $v(G)$ responses. For the same temperature increase, the shaded band in Figure 5 reflects the expected range of between-laboratory behavior. That is, if a first laboratory measures a $v(G)$ response at 25°C shown by the solid line, a second laboratory could measure a $v(G)$ response at 100°C anywhere within the

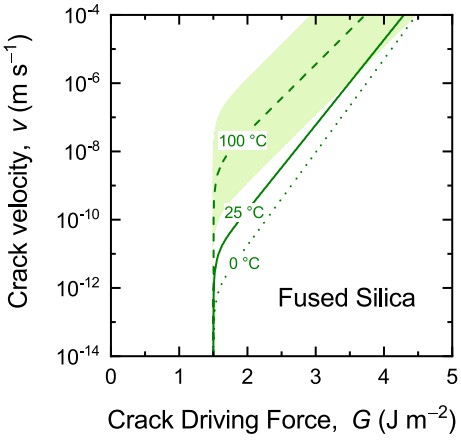

FIGURE 5 Best estimates (lines) and uncertainty (band) of crack velocity $v(G)$ behavior for fused silica in water at various temperatures based on analysis of published multi-laboratory data [Colour figure can be viewed at wileyonlinelibrary.com]

shaded band. Comparison of Figures 1 and 5 shows the multi-laboratory variation bands are comparable in magnitude. The lower, dotted, line in Figure 5 is for $T = 0°C$, freezing water. The crack velocity decreases, about a factor of 10, with decrease in temperature, reflecting decreased thermal activation. The dependence of the crack velocity on the mechanical energy release rate increases only weakly. A shaded band, similar to that shown, could be drawn around the $T = 0°C$ response, reflecting between-laboratory variability, although direct experimental measurements in freezing as opposed to cold water are unlikely. Overall, thermal activation effects in fused silica crack velocity responses are large, although arbitrary laboratory to laboratory comparisons could obscure the significance of temperature effects: The scale of the shaded band representing differences between observations in different laboratories is comparable to the extreme difference in crack velocity between freezing and boiling water.

4.2 | Time to failure behavior

Thermal activation effects in fracture-controlled reliability can be assessed from the influence of temperature on the time to failure of a stressed ceramic component. Detailed considerations of stress levels and flaw size distributions were made previously[1] but here attention is focused on temperature. If the stress on a component is such that the mechanical energy release rate on the failure controlling flaw is sufficiently far from the threshold, the time to failure, t_f, is given by

$$t_f = t_{ref} \exp\left[u_1/kT + u_0\left(1 - S^2\right)/2kT\right]/S^2. \quad (10)$$

Equation (10) uses the same $v(G)$ formulation and notation as above and (after some manipulation) isolates stress and temperature effects.[1] t_{ref} is a reference time that depends only on temperature invariant terms, including component and flaw geometry. S is the dimensionless ratio of the constant applied stress to the maximum, inert, strength of the flawed component, and therefore $S < 1$. Equation (10) makes clear that for fixed S increasing the temperature decreases time to failure (not considered here is that for fixed T, increasing S also decreases t_f).

Figure 6A is a plot of time to failure vs temperature using Equation (10). The failure and reference times have been set by using u_0 and u_1 from above and selecting the temperature invariant parameters such that $t_f = t_{ref} = 10^7$ s (about four months) at $T = 20°C$, indicated by the solid symbol. As the temperature is increased the time to failure decreases significantly, such that by 100°C the mean time to failure, indicated by the solid line, is about 2×10^4 seconds (about five hours). The shaded band in Figure 6A indicates uncertainty in the predicted lifetime arising from the uncertainties in u_0 and u_1. The exponential dependence on these parameters in Equation (10) leads to a factor of about 10 uncertainty in time to failure,

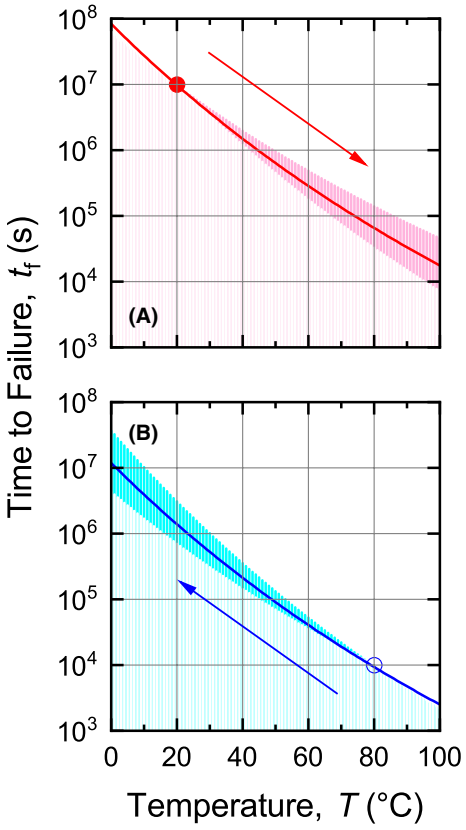

FIGURE 6 Best estimates of time to failure vs temperature for a fused silica component in water. (A) Increasing temperature prediction in direction of arrow from filled symbol. (B) Decreasing temperature prediction in direction of arrow from open symbol. Shaded bands represent failure time uncertainties arising from thermal activation energy uncertainty [Colour figure can be viewed at wileyonlinelibrary.com]

although the parameter uncertainties reflect relative multi-laboratory variability of only ±15%. Hence the decreased time to failure could vary from about 1 hour to about 1 day. There are two ways to interpret Figure 6A. The first is to recognize that component lifetime and thus reliability will be significantly truncated by increases in temperature. This places significant bounds on the use temperature (eg, do not load items by stacking in the hot dishwasher) or the useful lifetime (eg, use only for a temporary repair in a hot environment). The second interpretation is to recognize that accelerated testing at elevated temperature is viable for this fused silica component. Many tests of components could be completed in a few hours in boiling water to provide guidance for lifetimes of components intended for use over several weeks in lukewarm water.

Figure 6B is also a plot of time to failure vs temperature using Equation (10), but in this case the failure and reference times have been set such that $t_f = t_{ref} = 10^4$ seconds (about three hours) at $T = 80°C$, indicated by the open symbol. As the temperature is decreased here, the time to failure increases significantly, such that by 0°C the mean time to failure, indicated by the solid line, is about 10^7 seconds. The shaded band indicates

uncertainty in the prediction and again the exponential dependence on the energy parameters leads to about a factor of 10 uncertainty in time to failure and hence the increased time to failure could vary from about one month to about one year. The simplest way to interpret Figure 6B is that decreased temperature increases time to failure by freezing out crack propagation (eg, a cold fish tank will last longer). Careful examination of Figure 6 shows that the magnitudes of warming and cooling effects are not quite identical, but that even for the large thermal activation energy considered here the effect is slight.

In terms of advanced components, optical fibers, microelectronic devices, or MEMS, Figure 6 requires alteration in two ways. The first is that the shaded bands should be increased in size to reflect the convolution of component-specific flaw size distributions with the material variability portrayed. Figure 6 could then be used directly to address the effects of wet processes on yield in microelectronics or MEMS manufacturing. The second way that Figure 6 requires alteration is to recognize that reliability of advanced components should address times to failure of 10^8 seconds (about three years; lifetime of a microelectronics device) to 10^9 seconds (about 30 years; lifetime of an optical fiber or MEMS switch on a missile). Equation (10) shows that stress and temperature effects are not quite separable and so a reliability prediction cannot simply translate the curves of Figure 6 to account for smaller applied stresses operating over smaller temperature ranges and generate longer times to failure. A similar caveat applies to the separability of flaw size and temperature: optical fibers with ultrasmall flaws can exhibit different reliability degradation in water than bulk fused silica with well-defined cracks.[44] Finally, it should be recognized that a reliability prediction requires an estimate of failure *probability* within specified performance conditions, for example, time, temperature, stress.[1] Hence, Figures 1–5, culminating in Figure 6, provide a firm foundation for developing and validating such predictions.

5 | CONCLUSIONS

The temperature-independent nanoscale bond rupture parameters for fused silica in water, based on extensive analysis of published experimental crack velocity measurements, are

$$a = (0.218 \pm 0.016)\ \text{nm},$$

$$u_0 = (43 \pm 13)\ \text{kJ mol}^{-1}, \text{and}$$

$$u_1 = (69 \pm 11)\ \text{kJ mol}^{-1},$$

where value ± uncertainty represents multi-laboratory average ± variation. The macroscale temperature-dependent crack velocity is given in nanoscale terms by

$$v = (2kTa/h) \exp\left(-u_1/kT\right) \sinh\left[\left(Ga^2 - u_0\right)/2kT\right]/B,$$

where the first two terms represent kinetic effects and thermal activation, the third term represents the departure of the fracture system from equilibrium, and the fourth term represents the effects of geometry. An implication of the analysis is that the fracture surface energy characterizing thermodynamic equilibrium is $2\gamma = u_0/a^2 = 1.5\ \text{J m}^{-2}$. A new analysis was presented that eliminated dependence on the geometry term in evaluation of u_1, but which retained a critical dependence on the departure from equilibrium. The value resulting from the analysis was much greater than assumed in some previous works leading to crack velocity ranges of more than 10^2 for fracture of fused silica in freezing and boiling water. The effects of temperature on reliability of fused silica components were predicted to be large, with over a factor of 10^3 difference expected between times to failure of components in freezing and boiling water conditions.

ACKNOWLEDGMENTS

The author appreciates discussions with Drs. C.R. Kurkjian, M.J. Matthewson, and S.M. Wiederhorn on this subject over many years.

ORCID

Robert F. Cook https://orcid.org/0000-0003-0422-8881

REFERENCES

1. Cook RF. Long-term ceramic reliability analysis including the crack-velocity threshold and the "bathtub" curve. J Am Ceram Soc. 2018;101:5732–44.
2. Cook RF. Multi-scale effects in the strength of ceramics. J Am Ceram Soc. 2015;98:2933–47.
3. Lawn BR. An atomistic model of kinetic crack growth in brittle solids. J Mater Sci. 1975;10:469–80.
4. Cook RF, Liniger EG. Kinetics of indentation cracking in glass. J Am Ceram Soc. 1993;76:1096–105.
5. Cook RF. Environmentally-controlled non-equilibrium crack propagation in ceramics. Mater Sci Eng A. 1999;260:29–40.
6. Cook RF, Liniger EG. Stress-corrosion cracking of low dielectric-constant spin-on glass thin films. J Electrochem Soc. 1999;146:4439–48.
7. Hughey MP, Morris DJ, Cook RF, Bozeman SP, Kelly BL, Chakravarty S, et al. Four-point bend adhesion measurements of copper and permalloy systems. Engin Fracture Mech. 2004;71(2):245–61.
8. Rice JR. Thermodynamics of the quasi-static growth of Griffith cracks. J Mech Phys Solids. 1978;26:61–78.
9. Wiederhorn SM, Bolz LH. Stress corrosion and static fatigue of glass. J Am Ceram Soc. 1970;53:543–8.
10. Wiederhorn SM, Evans AG, Fuller ER, Johnson H. Application of fracture mechanics to space-shuttle windows. J Am Ceram Soc. 1974;57:319–23.
11. Sakaguchi S, Sawaki Y, Abe Y, Kawasaki T. Delayed failure in silica glass. J Mater. Sci. 1982;17:2878–86.

12. Michalske TA, Freiman SW. A molecular interpretation of stress corrosion in silica. Nature. 1982;295:511–2.
13. Michalske TA, Smith WL, Bunker BC. Fatigue mechanisms in high-strength silica-glass fibers. J Am Ceram Soc. 1991;74:1993–6.
14. Michalske TA, Bunker BC. A chemical kinetics model for glass fracture. J Am Ceram Soc. 1993;76:2613–8.
15. Michalske TA, Freiman SW. A molecular mechanism for stress corrosion in vitreous silica. J Am Ceram Soc. 1983;66:284–8.
16. Michalske TA, Bunker BC. Slow fracture model based on strained silicate structures. J Appl Phys. 1984;56:2686–93.
17. Hibino Y, Sakaguchi S, Tajima Y. Crack growth in silica glass under dynamic loading. J Am Ceram Soc. 1984;67:64–8.
18. Hibino Y, Sakaguchi S, Tajima Y. Crack growth in vitreous silica under dynamic loading. J Mater Sci Letters. 1983;2:388–92.
19. Muraoka M, Abe H. Subcritical crack growth in silica optical fibers in a wide range of crack velocities. J Am Ceram Soc. 1996;79:51–7.
20. Ritter JE, Fox JR, Hutko DI, Lardner TJ. Moisture-assisted crack growth at epoxy-glass interfaces. J Mater Sci. 1998;33:4581–8.
21. Wiederhorn SM. Fracture surface energy of glass. J Am Ceram Soc. 1969;52:99–105.
22. Lawn BR. Diffusion-controlled subcritical crack growth in the presence of a dilute gas environment. Mater Sci Engin. 1974;13:277–83.
23. Koike A, Tomozawa M. Fictive temperature dependence of subcritical crack growth rate of normal glass and anomalous glass. J Non-Cryst Solids. 2006;352:5522–30.
24. Koike A, Tomozawa M, Setsuro I. Sub-critical crack growth rate of soda-lime-silicate glass and less brittle glass as a function of fictive temperature. J Non-Cryst Solids. 2007;353:2675–80.
25. Hatty V, Kahn H, Heuer AH. Fracture toughness, fracture strength, and stress corrosion cracking of silicon dioxide thin films. J Microelectromechanical Systems. 2008;17:943–7.
26. Crichton SN, Tomozawa M, Hayden JS, Suratwala TI, Campbell JH. Subcritical crack growth in a phosphate laser glass. J Am Ceram Soc. 1999; 82:3097–104.
27. Chevalier J, Fantozzi G. Slow crack propagation in ceramics at the nano- and micro-scale: effect of the microstructure. In: Bradt RC, Munz D, Sakai M, White KW, editors. Fracture mechanics of ceramics. New York, NY: Springer Science+Business Media Inc; 2005: pp. 173–90.
28. Lane MW, Snodgrass JM, Dauskardt RH. Environmental effects on interfacial adhesion. Microelectron Reliab. 2001;41:1615–24.
29. Sglavo VM, Green DJ. Fatigue limit in fused silica. J Eur Ceram Soc. 2001;21:561–7.
30. Michalske TA, Fuller ER Jr. Closure and repropagation of healed cracks in silicate glass. J Am Ceram Soc. 1985;68:586–90.
31. Lawn BR, Roach DH, Thomson RM. Thresholds and reversibility in brittle cracks: an atomistic surface force model. J Mater Sci. 1987;22:4036–50.
32. Cook RF. Strength of brittle materials in moderately corrosive environments. J Am Ceram Soc. 2018;101:1684–95.
33. Glaesemann GS. High speed strength testing of optical fibers. In: Yuce HH, Paul DK, Greenwell RA, editors. Optical network engineering and integrity. Bellingham, WA: SPIE; 1996: pp. 38–44.
34. Semjonov SL, Glaesemann GS, Clark DA, Bubnov MM. Fatigue behavior of silica fibers with different defects. In: Optical fibers and fiber component mechanical reliability and testing. Matthewson MJ, editor. Bellingham, WA: SPIE; 2001: pp. 28–35.
35. Shiue YS, Matthewson MJ. Apparent activation energy of fused silica optical fibers in static fatigue in aqueous environments. J Eur Ceram Soc. 2002;22:2325–32.
36. Fisk GA, Michalske TA. Laser-based and thermal studies of stress corrosion in vitreous silica. J Appl Phys. 1985;58:2736–41.
37. Chandan HC, Kalish D. Temperature dependence of static fatigue of optical fibers coated with a UV-curable polyurethane acrylate. J Am Ceram Soc. 1982;65:171–3.
38. Ritter JE Jr, Sullivan JM Jr, Jakus K. Application of fracture-mechanics theory to fatigue failure of optical glass fibers. J Appl Phys. 1978;49:4779–82.
39. Ritter JE Jr, Jakus K, Babinski RC. Effect of temperature and humidity on delayed failure of optical fibers. In: Methods for assessing the structural reliability of brittle materials. Freiman S, Michael H, editors. West Conshohocken, PA: ASTM International; 1984: pp. 131–41.
40. Ritter JE Jr, Glaesemann GS, Jakus K. Effect of temperature on the strength and fatigue behavior of optical fibers. J Mater Sci. 1984;19:4087–92.
41. Sakaguchi S, Kimura T. Influence of temperature and humidity on dynamic fatigue of optical fibers. J Am Ceram Soc. 1981;64:259–62.
42. Matthewson MJ, Kurkjian CR, Haines CD, Venugopal N. Temperature dependence of strength and fatigue of fused silica fiber in the range 77 to 473 K. In: Reliability of optical fiber components, devices, systems, and networks. Limberger HG, Matthewson MJ, editors. Bellingham, WA: SPIE; 2003: pp. 74–9.
43. Gerberich WW, Stout M. Discussion of thermally activated approaches to glass fracture. J Am Ceram Soc. 1976;59:222–5.
44. Glaesemann GS. The mechanical behavior of large flaws in optical fiber and their role in reliability predictions. In Proceedings 41st International Wire and Cable Symposium. Eatontown, NJ: IWCS; 1992: pp. 698–704.

How to cite this article: Cook RF. Thermal activation effects in crack propagation and reliability of fused silica. *J Am Ceram Soc*. 2019;102:7575–7583. https://doi.org/10.1111/jace.16661